Porous and Low-Crystalline Manganese Silicate Hollow Spheres Wired by Graphene Oxide for High-Performance Lithium and Sodium Storage

Jiexin Zhu,[†] Chunjuan Tang,[*,†,‡] Zechao Zhuang,[†] Changwei Shi,[†] Narui Li,[†] Liang Zhou,[†] and Liqiang Mai[*,†,§]

[†] State Key Laboratory of Advanced Technology for Materials Synthesis and Processing, International School of Materials Science and Engineering, Wuhan University of Technology, Wuhan 430070, Hubei, P. R. China

[‡] Department of Mathematics and Physics, Luoyang Institute of Science and Technology, Luoyang 471023, P. R. China

[§] Department of Materials Science and Engineering, University of California at Los Angeles, Los Angeles, California 90095-6989, United States

ⓢ Supporting Information

ABSTRACT: Herein, a graphene oxide (GO)-wired manganese silicate (MS) hollow sphere (MS/GO) composite is successfully synthesized. Such an architecture possesses multiple advantages in lithium and sodium storage. The hollow MS structure provides a sufficient free space for volume variation accommodation; the porous and low-crystalline features facilitate the diffusion of lithium ions; meanwhile, the flexible GO sheets enhance the electronic conductivity of the composite to a certain degree. When applied as the anode material for lithium-ion batteries (LIBs), the as-obtained MS/GO composite exhibits a high reversible capacity, ultrastable cyclability, and good rate performance. Particularly, the MS/GO composite delivers a high capacity of 699 mA h g^{-1} even after 1000 cycles at 1 A g^{-1}. The sodium-storage performance of MS/GO has been studied for the first time, and it delivers a stable capacity of 268 mA h g^{-1} after 300 cycles at 0.2 A g^{-1}. This study suggests that the rational design of metal silicates would render them promising anode materials for LIBs and SIBs.

KEYWORDS: hollow sphere, manganese silicate, graphene oxide, low-crystalline, lithium-ion battery, sodium-ion battery
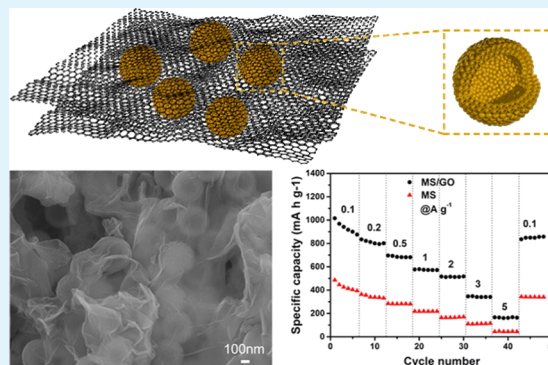
INTRODUCTION

Since their commercialization, lithium-ion batteries (LIBs) have dominated the market of power sources for portable electronics because of their high energy density and good cycling stability.[1−5] However, the performances of current state-of-the-art LIBs, such as energy density, power density, safety, and cycle life, cannot meet the ever-increasing demands of electric vehicles and smart grids. Therefore, significant efforts have been dedicated to the development of novel high-capacity electrode materials.[6−11]

Recently, metal silicates have been recognized as a promising family of high-capacity anode materials.[12−20] For example, nickel silicate is reported as an LIB's anode, with a high initial discharge capacity of 1650 mA h g^{-1}.[18] Mueller et al. reported a cobalt silicate anode with a reversible capacity of ∼600 mA h g^{-1}; however, the cycling and rate performances of the material are unsatisfactory due to its large particle size.[19] To boost the cyclability and rate capability, an effective strategy is compositing metal silicate with conductive carbon.[12−17,20] Jin et al. designed a sandwich-structured graphene−nickel silicate−nickel ternary composite.[15] Qu et al. fabricated a composite of

layered zinc silicate/carbon/reduced graphene oxide (RGO).[16] Both composites show enhanced cycling stability and rate performance. Another effective way to boost the electrochemical performance of metal silicates is constructing nanostructures.[12,13,18,20,21] The rationally designed nanostructures can shorten the diffusion length of lithium ions, ensure a sufficient electrode/electrolyte contact, and reduce the strain induced by repeated lithiation/delithiation.[22] With a sufficient free space for volume variation accommodation and strain relaxation, the hollow sphere has been demonstrated to be one of the most attractive nanostructures for electrode materials.[14,17,23−28] For example, when coupled with RGO, nickel silicate and copper silicate hollow spheres can serve as long-life anode materials for LIBs.[14,17]

Recently, amorphous and low-crystalline electrode materials have attracted a great attention in electrochemical energy storage and conversion.[29−40] Compared to their highly
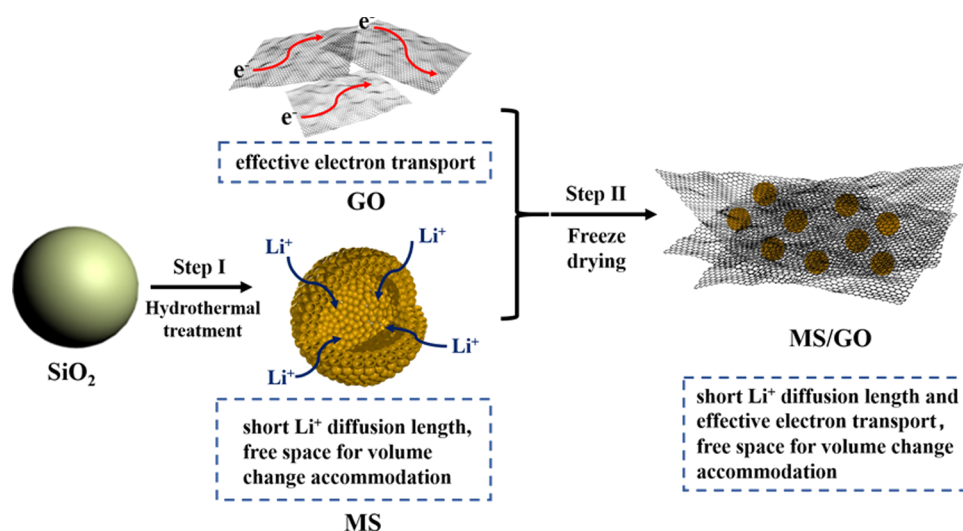
Figure 1. Schematic illustration of the synthesis of pristine MS and MS/GO composite. Step I: hydrothermal synthesis of MS hollow spheres from Stöber SiO_2 spheres. Step II: assembling the MS hollow spheres and GO nanosheets into MS/GO nanocomposite via freeze drying.

crystalline counterparts, the amorphous and low-crystalline electrode materials are more effective in lithium-ion diffusion and strain relaxation.[32−34,37,38] As an excellent example, amorphous $FePO_4$ has been demonstrated to be a superior cathode material for both lithium and sodium storage.[29−31] In addition, both amorphous and low-crystalline FeOOH can function as high-performance pseudocapacitive electrode materials in supercapacitors.[39,40] Through a comparative study, Zhao et al. demonstrated that the amorphous copper vanadate outperforms its highly crystalline counterpart in lithium storage.[38] For metal silicate, it has also been demonstrated that the amorphous cobalt silicate, when composited with carbon, can deliver outstanding electrochemical performance.[12] It should be pointed out that all of the above-mentioned amorphous/low-crystalline electrode materials have poor electronic conductivity, which is unfavorable for electron conduction. Therefore, conductive carbon is usually introduced in the electrode materials to enhance their electrochemical performances.[30,32,38]

Herein, we report for the first time a facile two-step synthesis of the low-crystalline manganese silicate hollow sphere/graphene oxide (MS/GO) composite. With a porous and low-crystalline wall for a fast lithium-ion diffusion, a hollow interior for volume change accommodation, and a GO network for electron conduction, the as-obtained MS/GO composite manifests an excellent lithium-storage performance. In addition, this is the first report on applying metal silicate/GO as the anode material for SIBs.

■ RESULTS AND DISCUSSION

The synthesis of MS/GO involves two major steps (Figure 1). In step I, porous and low-crystalline manganese silicate (MS) hollow spheres are synthesized via a facile hydrothermal method, in which Stöber SiO_2 spheres are used as the sacrificial templates, $MnCl_2·4H_2O$ is used as the Mn source, and NH_4Cl and $NH_3·H_2O$ are used to adjust the pH value. In step II, the MS hollow spheres and GO are dispersed in water and freeze-dried to construct the MS/GO composite. For comparison, an MS/RGO composite is also prepared by annealing the as-obtained MS/GO at 700 °C for 10 h in Ar/H_2 (95%/5%).

X-ray diffraction (XRD) patterns of the as-obtained MS and MS/GO (Figure 2) show three weak and broad diffraction
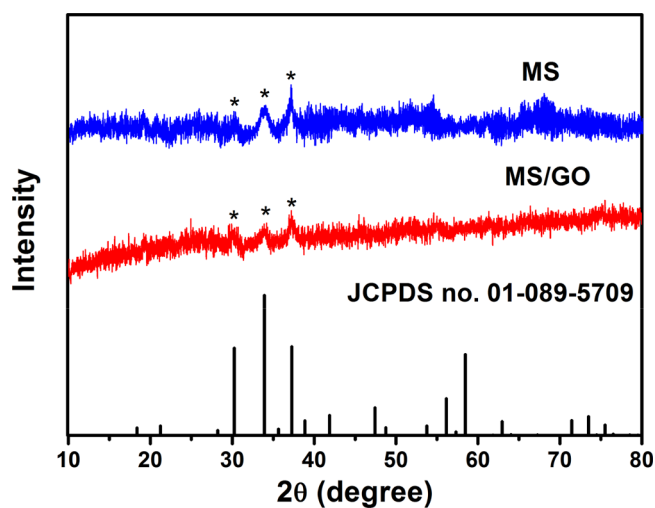
Figure 2. XRD patterns of the pristine MS and the MS/GO composite.

peaks, indicating the low-crystalline nature of the products. Both patterns can be indexed to $Mn_3(II)Mn_2(III)(SiO_4)_3$ (JCPDS card no. 01-089-5709). No diffraction peaks for GO can be detected in the XRD pattern of the MS/GO composite, which is due to the ultrathin feature and low content of GO in the composite.[20,41]

The existence and content of GO in the MS/GO composite are determined by Raman spectroscopy and thermogravimetric analysis (TGA). The Raman spectrum (Figure S1) presents two obvious carbon bands. The D band at 1323 cm^{-1} is due to the defects, whereas the G band at 1589 cm^{-1} is ascribed to the in-plane vibration of sp^2 carbon atoms.[42] The I_D/I_G ratios for MS/RGO and MS/GO are determined to be 0.94 and 1.0, respectively. The close I_D/I_G ratios indicate that the graphitization degrees of MS/RGO and MS/GO are similar. The GO content is determined to be 5.8 wt % by TGA (Figure S2). The slight weight loss of pristine MS can be ascribed to the elimination of moisture.
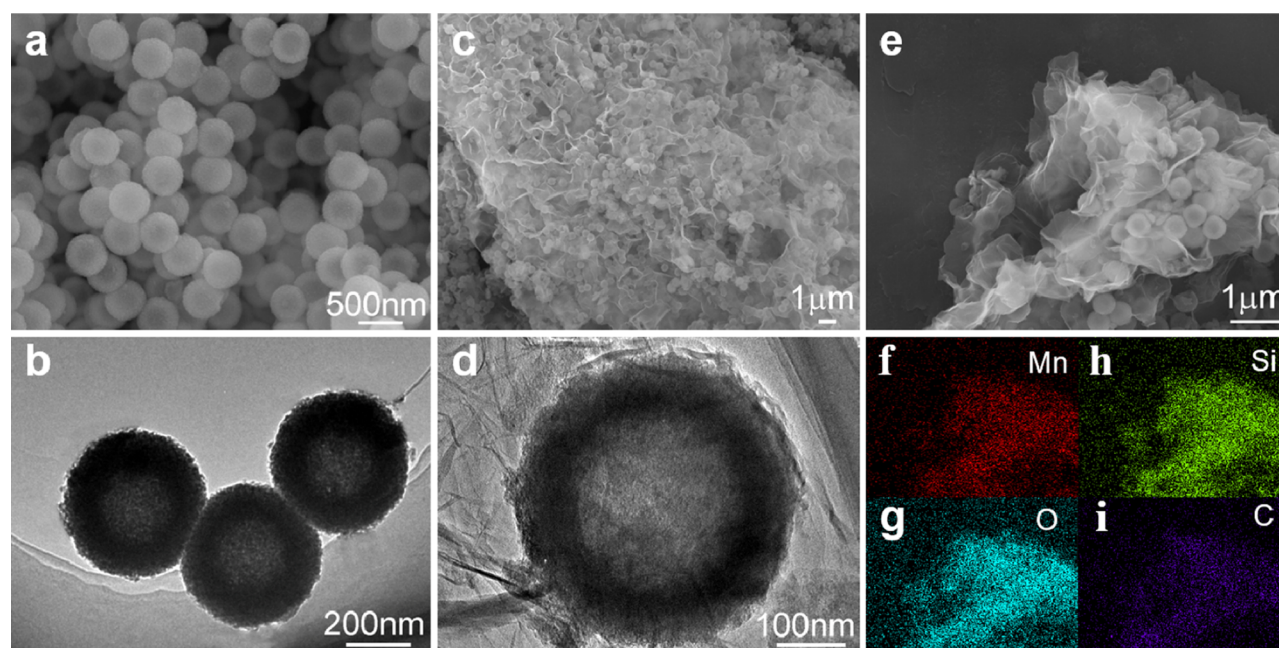
Figure 3. FESEM (a) and TEM (b) images of MS, FESEM (c) and TEM (d) images of MS/GO, and element-mapping results of MS/GO (e−i).
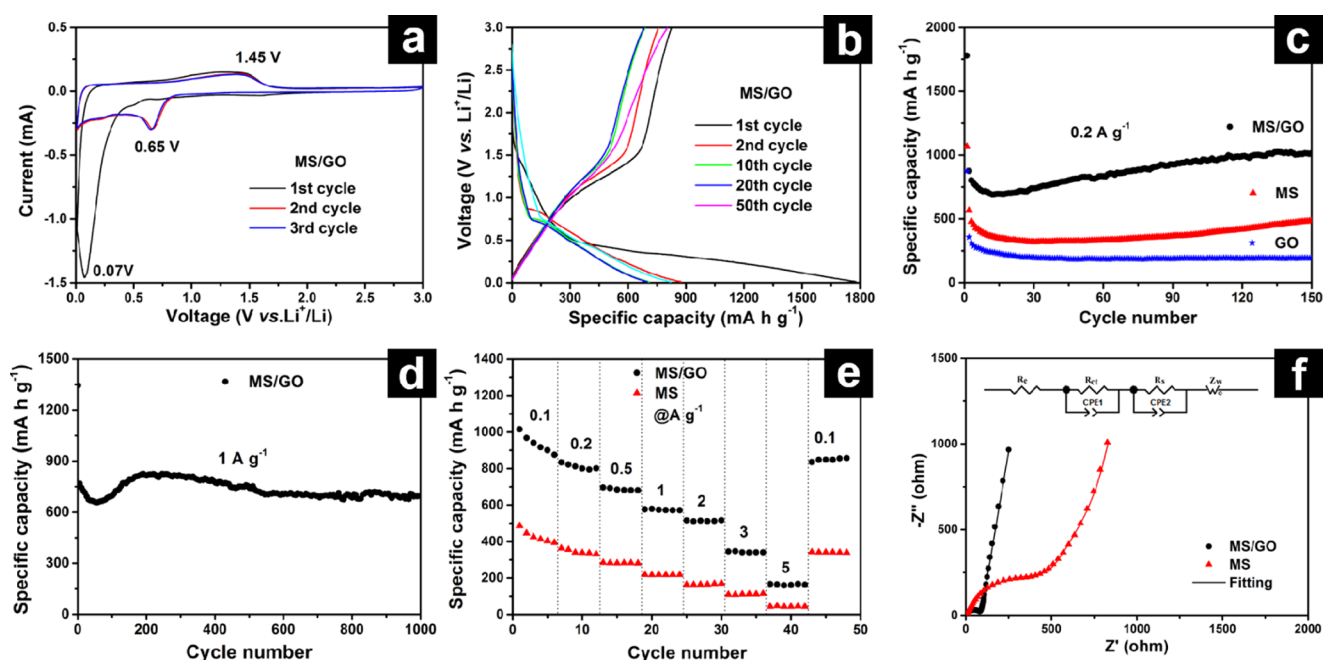
Figure 4. CV curves of MS/GO (a); representative discharge−charge curves of MS/GO at the current density of 0.2 A g^{-1} (b); cycling performances of MS/GO, pristine MS, and GO at 0.2 A g^{-1} (c); cycling performance of MS/GO at 0.5 A g^{-1} (d); rate performances of MS/GO and pristine MS (e); and Nyquist plots of MS/GO and pristine MS, where R_e = external resistance, R_{ct} = charge-transfer resistance, CPE = constant phase element, R_s = SEI resistance, and Z_w = Warburg impedance (f).

The nanoporous features of MS and MS/GO are characterized by nitrogen sorption (Figure S3). Both samples possess high specific surface areas and abundant mesopores. The Brunauer−Emmett−Teller surface areas of MS and MS/GO are determined to be 365 and 325 m^2 g^{-1}, respectively. The pore sizes of both samples are centered at approximately 2 nm. Such a highly porous feature is desirable in lithium storage as it can facilitate the ion diffusion.

The morphology and microstructure of the MS/GO composite, pristine MS, and the sacrificing template are studied by field emission scanning electron microscopy (FESEM) and transmission electron microscopy (TEM). The sacrificing template, namely, Stöber SiO$_2$, is composed of monodisperse microspheres with smooth surface (Figure S4). The diameter of the SiO$_2$ spheres is ∼400 nm. After the hydrothermal treatment, the Stöber SiO$_2$ is converted into MS. The MS is composed of microspheres with rough surface and a diameter of ∼450 nm (Figure 3a). The TEM image (Figure 3b) demonstrates the hollow structure of MS. The thickness of the shell is determined to be approximately 120 nm. From the high-magnification TEM images (Figure S5), it can be observed that the shell of MS is composed of nanobubbles with
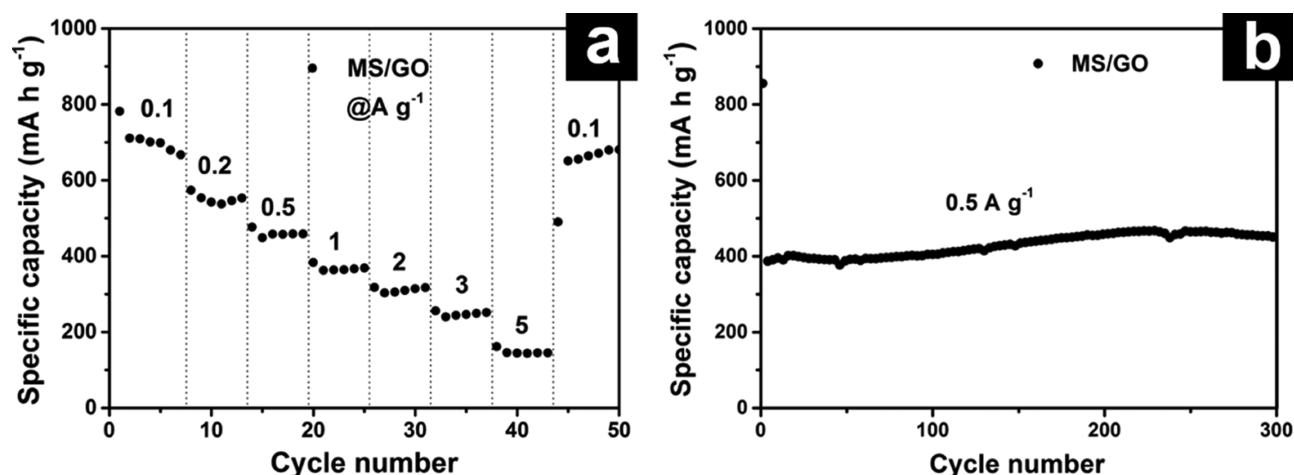
Figure 5. Rate performance (a) and cycling performance (b) of MS/GO at 0 °C.

diameters of ∼2 nm, which is consistent with the literature.[43] The element-mapping analysis (Figure S6) shows that the Mn, Si, and O elements distributed homogeneously in the MS hollow spheres. Figure 3c,d shows the FESEM and TEM images of the MS/GO composite, respectively. It can be observed that the GO forms a continuous network and the MS hollow spheres are well dispersed in it. The element-mapping results (Figure 3e–i) indicate the homogeneous distribution of Mn, Si, O, and C in the MS/GO composite.

Figure 4a presents the initial three cyclic voltammetry (CV) curves of the MS/GO at a scan rate of 0.1 mV s^{-1}. An intense reduction peak can be observed at around 0.07 V in the first cathodic process, which is caused by the initial lithiation and the formation of a solid electrolyte interphase (SEI) layer on the electrode surface.[13,17] In the second cathodic scan, the peak shifts to approximately 0.65 V, and this new peak is ascribed to the reversible lithium-ion insertion into the MS/GO.[44] In the anodic sweeps, an oxidation peak located at about 1.45 V can be observed, corresponding to the lithium extraction. The CV curves of pristine MS are similar to those of MS/GO (Figure S7), suggesting their identical reaction mechanism.

Figure 4b shows representative discharge–charge curves of the MS/GO composite at 0.2 A g^{-1}. The discharge plateau is between 0.01 and 0.75 V, and the charge plateau is located at 1.0–1.5 V. The charge plateau is a little high for practical application; however, this is a common issue for conversion-reaction-based anode materials.[45] The MS/GO composite delivers initial discharge and charge capacities of 1780 and 825 mA h g^{-1}, respectively. The corresponding coulombic efficiency is 46.3%, and the irreversible capacity is as high as 955 mA h g^{-1}. The large capacity loss is ascribed to the initial irreversible electrochemical reaction as well as the formation of SEI.[15,17] This phenomenon is very common for anode materials based on conversion and alloying/dealloying reactions.[46–48] Although the initial coulombic efficiency of MS/GO (46.3%) is lower than that of commercial anode materials, it can be improved by employing prelithiation.[49,50]

Figure 4c displays the cycling performances of the MS/GO composite, pristine MS, and GO at the current density of 0.2 A g^{-1}. The MS/GO composite delivers a much higher capacity than the pristine MS and GO. A stable capacity of 1015 mA h g^{-1} can be achieved after 150 cycles. It is worth noting that the capacity undergoes a progressive increasing process after 15 cycles. A similar phenomenon has been reported in manganese

oxide-based anodes, and it may originate from the oxidation of Mn^{2+} to Mn^{4+} at a high charge voltage.[51–53] Under similar conditions, the pristine MS delivers a capacity of 484 mA h g^{-1}, whereas the GO delivers a capacity of only 196 mA h g^{-1}. The synergetic effect of MS hollow spheres and GO is responsible for the high specific capacity and excellent cycling stability of MS/GO. Although MS possesses a high theoretical capacity of 1226 mA h g^{-1}, the active material utilization is low due to its poor electronic conductivity. At 0.2 A g^{-1}, the pristine MS delivers a moderate reversible capacity of 484 mA h g^{-1}. With the introduction of GO, both the electronic conductivity and specific capacity of MS can be enhanced significantly.

At a current density of 1 A g^{-1}, the MS/GO composite delivers a reversible capacity of 828 mA h g^{-1}, maintaining 699 mA h g^{-1} after 1000 cycles (Figure 4d). At an even higher current density of 2 A g^{-1}, the MS/GO composite manifests a capacity of 445 mA h g^{-1} after 1000 cycles, confirming its desirable cycling stability (Figure S8). Reducing the GO to RGO improves the cycling stability while slightly sacrificing the reversible capacity; the MS/RGO composite manifests a very stable capacity of ∼674 mA h g^{-1} at 1 A g^{-1} (Figure S9).

To evaluate the structural stability, the morphology of MS/GO after 500 cycles at 1 A g^{-1} is investigated (Figure S10). Both the MS spheres and GO nanosheets can be well retained after cycling, demonstrating the excellent structural stability of MS/GO. Such an excellent structural stability can be attributed to the volume change buffering ability of the MS hollow structure and the flexibility of GO.

Rate performance is one of the most important parameters for evaluating electrode materials. Figure 4e presents the rate performances of MS/GO and pristine MS. The MS/GO composite delivers average capacities of 936, 811, 686, 574, 514, 343, and 164 mA h g^{-1} at current densities of 0.1, 0.2, 0.5, 1, 2, 3, and 5 A g^{-1}, respectively. When the current density is returned to 0.1 A g^{-1}, the capacity resumes to 850 mA h g^{-1}, which is ∼90.8% of the initial capacity. No matter what the current density is, the pristine MS delivers a much lower capacity than the MS/GO composite. The superior performance of MS/GO over pristine MS in terms of specific capacity and rate capability suggests that the GO is beneficial to the reactivity and conductivity of MS. Compared to previous reports on MS anode materials,[21,54] the MS/GO composite reported here shows the highest specific capacity and cycling stability.
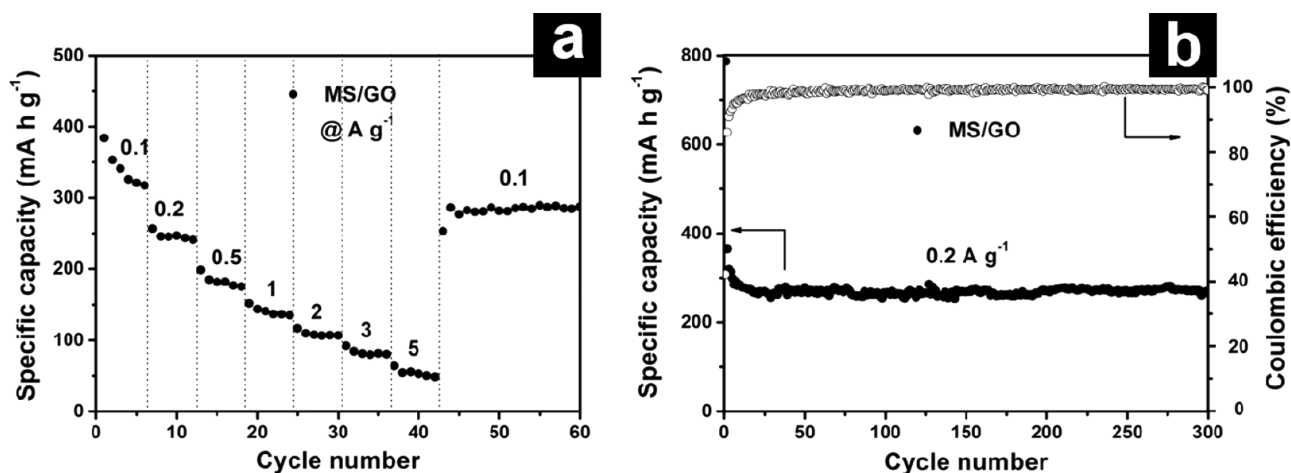
Figure 6. Rate performance (a), cycling performance and coulombic efficiency (b) of MS/GO for sodium storage.

To evaluate the reaction kinetics of MS/GO and MS electrodes, electrochemical impedance spectra are recorded. The Nyquist plots of both MS/GO and MS electrodes consist of a semicircle at the high-frequency region and a slope line at the low-frequency region (Figure 4f). The semicircle represents the charge-transfer impedance (R_{ct}), whereas the slope line represents the Warburg impedance related to solid-state Li$^+$ diffusion. The R_{ct} value of MS/GO is determined to be 78.52 Ω, which is much lower than that of pristine MS (175.6 Ω). This suggests that the MS/GO composite has a much faster charge-transfer process than the pristine MS. The low-frequency line for MS/GO is much steeper than that of MS, indicating the much faster Li$^+$ diffusion in MS/GO. The enhanced Li$^+$ diffusion can be attributed to the fact that the introduction of GO nanosheets induces the formation of a less aggregated structure with more interspaces. Reducing the GO to RGO decreases the R_{ct} from 78.52 Ω for MS/GO to 51.7 Ω for MS/RGO (Figure S11).

For practical applications, low-temperature performance is another important parameter for electrode materials. The low-temperature lithium-storage performances of MS/GO at 0 °C are presented in Figure 5. It delivers average capacities of 707, 551, 460, 368, 311, 248, and 148 mA h g^{-1} at current densities of 0.1, 0.2, 0.5, 1, 2, 3, and 5 A g^{-1}, respectively (Figure 5a). The MS/GO composite also exhibits an excellent low-temperature cycling performance (Figure 5b). A capacity of 425 mA h g^{-1} can be obtained after 300 cycles at 0.5 A g^{-1}.

The abundance and low cost of sodium make the SIBs a promising alternative to LIBs.[13,30,31,55,56] Although sodium has a number of features similar to those of lithium, most of the electrode materials for LIBs are not suitable for SIBs because of the large ionic radius of sodium. Considering that the porous and low-crystalline features may favor the insertion/extraction of Na$^+$, the sodium-storage performances of MS/GO are further studied. As shown in Figure 6a, the MS/GO composite delivers an average capacity of 340 mA h g^{-1} at a low current density of 0.1 A g^{-1}. Even at a high current density of 3 A g^{-1}, a capacity of 83.3 mA h g^{-1} can be retained. Figures S12 and 6b depict the representative discharge–charge curves and cycling performance of MS/GO at 0.2 A g^{-1}. It shows initial and second discharge capacities of 787 and 366 mA h g^{-1}, respectively. From the second cycle onward, it exhibits a good cycling stability and retains 268 mA h g^{-1} after 300 cycles and the coulombic efficiency is close to 100%. There are few

reports on using silicate as anode materials for SIBs. Gui et al. reported a CNT@NiSiO$_x$ anode with an initial capacity of 576 mA h g^{-1}; however, the capacity decays rapidly to only 213 mA h g^{-1} after 16 cycles at 20 mA g^{-1}.[13] This work proves that the porous and low-crystalline MS/GO composite is a potential anode material for SIBs.

CONCLUSIONS

In conclusion, a MS/GO composite has been successfully constructed. The as-prepared MS/GO composite exhibits a high lithium-storage capacity (825 mA h g^{-1} at 0.2 A g^{-1}), an excellent cyclability (699 mA h g^{-1} after 1000 cycles at 0.5 A g^{-1}), and a good rate performance. The excellent lithium-storage performance can be attributed to the porous and low-crystalline features for rapid lithium-ion diffusion, hollow structure for volume variation accommodation, and GO for electronic conduction. This work suggests that the rational design of metal silicate structures would render them promising anode materials for LIBs and SIBs.

ASSOCIATED CONTENT

Ⓢ Supporting Information

The Supporting Information is available free of charge on the ACS Publications website at DOI: 10.1021/acsami.7b06088.

> Experimental section containing synthesis of MS/GO, material characterizations, and electrochemical measurements; Raman spectra of MS/GO and MS/RGO; TGA curves of MS/GO and pristine MS; nitrogen adsorption−desorption isotherms and the corresponding pore size distributions of MS/GO and MS; SEM images of SiO$_2$ spheres; TEM images of MS; element-mapping result of MS; CV curve of MS; cycling performance and coulombic efficiency of MS/GO at a current density of 2 A g^{-1}; cycling performance of MS/RGO at a current density of 1 A g^{-1}; Nyquist plots of MS/GO and MS/RGO (PDF)

AUTHOR INFORMATION

Corresponding Authors
*E-mail: tangchunjuan@163.com (C.T.).
*E-mail: mlq518@whut.edu.cn (L.M.).
ORCID Ⓘ
Liqiang Mai: 0000-0003-4259-7725

Notes

■ REFERENCES

(1) Zhao, Y.; Han, C.; Yang, J.; Su, J.; Xu, X.; Li, S.; Xu, L.; Fang, R.; Jiang, H.; Zou, X.; Song, B.; Mai, L.; Zhang, Q. Stable Alkali Metal Ion Intercalation Compounds as Optimized Metal Oxide Nanowire Cathodes for Lithium Batteries. *Nano Lett.* **2015**, *15*, 2180−2185.

(2) Taberna, P. L.; Mitra, S.; Poizot, P.; Simon, P.; Tarascon, J. M. High Rate Capabilities Fe₃O₄-Based Cu Nano-Architectured Electrodes for Lithium-Ion Battery Applications. *Nat. Mater.* **2006**, *5*, 567−573.

(3) Liu, H.; Li, W.; Shen, D.; Zhao, D.; Wang, G. Graphitic Carbon Conformal Coating of Mesoporous TiO₂ Hollow Spheres for High-Performance Lithium Ion Battery Anodes. *J. Am. Chem. Soc.* **2015**, *137*, 13161−13166.

(4) Xu, Y.; Lin, Z.; Zhong, X.; Papandrea, B.; Huang, Y.; Duan, X. Solvated Graphene Frameworks as High-Performance Anodes for Lithium-Ion Batteries. *Angew. Chem., Int. Ed.* **2015**, *54*, 5345−5350.

(5) An, Q.; Xiong, F.; Wei, Q.; Sheng, J.; He, L.; Ma, D.; Yao, Y.; Mai, L. Nanoflake-Assembled Hierarchical Na₃V₂(PO₄)₃/C Microflowers: Superior Li Storage Performance and Insertion/Extraction Mechanism. *Adv. Energy Mater.* **2015**, *5*, No. 1401963.

(6) Yao, Y.; Liu, N.; McDowell, M. T.; Pasta, M.; Cui, Y. Improving the Cycling Stability of Silicon Nanowire Anodes with Conducting Polymer Coatings. *Energy Environ. Sci.* **2012**, *5*, 7927−7930.

(7) Zhang, H.; Zhou, L.; Noonan, O.; Martin, D.; Whittaker, A.; Yu, C. Tailoring the Void Size of Iron Oxide@Carbon Yolk-Shell Structure for Optimized Lithium Storage. *Adv. Funct. Mater.* **2014**, *24*, 4337−4342.

(8) Zhao, Y.; Feng, J.; Liu, X.; Wang, F.; Wang, L.; Shi, C.; Huang, L.; Feng, X.; Chen, X.; Xu, L.; Yan, M.; Zhang, Q.; Bai, X.; Wu, H.; Mai, L. Self-Adaptive Strain-Relaxation Optimization for High-Energy Lithium Storage Material through Crumpling of Graphene. *Nat. Commun.* **2014**, *5*, No. 4565.

(9) Sheng, J.; Li, Q.; Wei, Q.; Zhang, P.; Wang, Q.; Lv, F.; An, Q.; Chen, W.; Mai, L. Metastable Amorphous Chromium-vanadium Oxide Nanoparticles with Superior Performance as a New Lithium Battery Cathode. *Nano Res.* **2014**, *7*, 1604−1612.

(10) Zhou, X.; Yin, Y.-X.; Cao, A.-M.; Wan, L.-J.; Guo, Y.-G. Efficient 3D Conducting Networks Built by Graphene Sheets and Carbon Nanoparticles for High-Performance Silicon Anode. *ACS Appl. Mater. Interfaces* **2012**, *4*, 2824−2828.

(11) Liu, X.; Du, Y.; Hu, L.; Zhou, X.; Li, Y.; Dai, Z.; Bao, J. Understanding the Effect of Different Polymeric Surfactants on Enhancing the Silicon/Reduced Graphene Oxide Anode Performance. *J. Phys. Chem. C* **2015**, *119*, 5848−5854.

(12) Cheng, W.; Rechberger, F.; Ilari, G.; Ma, H.; Lin, W. I.; Niederberger, M. Amorphous Cobalt Silicate Nanobelts@carbon Composites as a Stable Anode Material for Lithium Ion Batteries. *Chem. Sci.* **2015**, *6*, 6908−6915.

(13) Gui, C. X.; Hao, S. M.; Liu, Y.; Qu, J.; Yang, C.; Yu, Y.; Wang, Q. Q.; Yu, Z. Z. Carbon Nanotube@layered Nickel Silicate Coaxial Nanocables as Excellent Anode Materials for Lithium and Sodium Storage. *J. Mater. Chem. A* **2015**, *3*, 16551−16559.

(14) Wei, X.; Tang, C.; Wang, X.; Zhou, L.; Wei, Q.; Yan, M.; Sheng, J.; Hu, P.; Wang, B.; Mai, L. Copper Silicate Hydrate Hollow Spheres Constructed by Nanotubes Encapsulated in Reduced Graphene Oxide as Long-Life Lithium-Ion Battery Anode. *ACS Appl. Mater. Interfaces* **2015**, *7*, 26572−26578.

(15) Jin, R.; Yang, Y.; Li, Y.; Liu, X.; Xing, Y.; Song, S.; Shi, Z. Sandwich-Structured Graphene-Nickel Silicate-Nickel Ternary Composites as Superior Anode Materials for Lithium-Ion Batteries. *Chem. − Eur. J.* **2015**, *21*, 9014−9017.

(16) Qu, J.; Yan, Y.; Yin, Y. X.; Guo, Y. G.; Song, W. G. Improving the Li-Ion Storage Performance of Layered Zinc Silicate through the Interlayer Carbon and Reduced Graphene Oxide Networks. *ACS Appl. Mater. Interfaces* **2013**, *5*, 5777−5782.

(17) Tang, C.; Sheng, J.; Xu, C.; Khajehbashi, S.; Wang, X.; Hu, P.; Wei, X.; Wei, Q.; Zhou, L.; Mai, L. Facile Synthesis of Reduced Graphene Oxide Wrapped Nickel Silicate Hierarchical Hollow Spheres for Long-Life Lithium-Ion Batteries. *J. Mater. Chem. A* **2015**, *3*, 19427−19432.

(18) Yang, Y.; Liang, Q.; Li, J.; Zhuang, Y.; He, Y.; Bai, B.; Wang, X. Ni₃Si₂O₅(OH)₄ Multi-Walled Nanotubes with Tunable Magnetic Properties and Their Application as Anode Materials for Lithium Batteries. *Nano Res.* **2011**, *4*, 882−890.

(19) Mueller, F.; Bresser, D.; Minderjahn, N.; Kalhoff, J.; Menne, S.; Krueger, S.; Winter, M.; Passerini, S. Cobalt Orthosilicate as a New Electrode Material for Secondary Lithium-Ion Batteries. *Dalton Trans.* **2014**, *43*, 15013−15021.

(20) Tang, C.; Zhu, J.; Wei, X.; He, L.; Zhao, K.; Xu, C.; Zhou, L.; Wang, B.; Sheng, J.; Mai, L. Copper Silicate Nanotubes Anchored on Reduced Graphene Oxide for Long-Life Lithium-Ion Battery. *Energy Storage Mater.* **2017**, *7*, 152−156.

(21) Wang, Y. Y.; Li, T.; Qi, Y. X.; Bai, R. L.; Yin, L. W.; Li, H.; Lun, N.; Bai, Y. J. Carbon-Coated Manganese Silicate Exhibiting Excellent Rate Performance and High-Rate Cycling Stability for Lithium-Ion Storage. *Electrochim. Acta* **2015**, *186*, 572−578.

(22) Martinet, S. Nanomaterials for Rechargeable Lithium Battery. *Nanomaterials for Sustainable Energy*; Springer International Publishing, 2016; pp 471−512.

(23) Xu, S.; Hessel, C. M.; Ren, H.; Yu, R.; Jin, Q.; Yang, M.; Zhao, H.; Wang, D. α-Fe₂O₃ Multi-Shelled Hollow Microspheres for Lithium Ion Battery Anodes with Superior Capacity and Charge Retention. *Energy Environ. Sci.* **2014**, *7*, 632−637.

(24) Wu, R.; Qian, X.; Yu, F.; Liu, H.; Zhou, K.; Wei, J.; Huang, Y. MOF-Templated Formation of Porous CuO Hollow Octahedra for Lithium-Ion Battery Anode Materials. *J. Mater. Chem. A* **2013**, *1*, 11126−11129.

(25) Zhou, L.; Zhuang, Z.; Zhao, H.; Lin, M.; Zhao, D.; Mai, L. Intricate Hollow Structures: Controlled Synthesis and Applications in Energy Storage and Conversion. *Adv. Mater.* **2017**, *29*, No. 1602914.

(26) Yan, C.; Chen, G.; Zhou, X.; Sun, J.; Lv, C. Template-Based Engineering of Carbon-Doped Co₃O₄ Hollow Nanofibers as Anode Materials for Lithium-Ion Batteries. *Adv. Funct. Mater.* **2016**, *26*, 1428−1436.

(27) Sun, X.; Zhang, H.; Zhou, L.; Huang, X.; Yu, C. Polypyrrole-Coated Zinc Ferrite Hollow Spheres with Improved Cycling Stability for Lithium-Ion Batteries. *Small* **2016**, *12*, 3732−3737.

(28) Sun, C.; Yang, J.; Rui, X.; Zhang, W.; Yan, Q.; Chen, P.; Huo, F.; Huang, W.; Dong, X. MOF-Directed Templating Synthesis of a Porous Multicomponent Dodecahedron with Hollow Interiors for Enhanced Lithium-Ion Battery Anodes. *J. Mater. Chem. A* **2015**, *3*, 8483−8488.

(29) Lee, Y. J.; Yi, H.; Kim, W. J.; Kang, K.; Yun, D. S.; Strano, M. S.; Ceder, G.; Belcher, A. M. Fabricating Genetically Engineered High-Power Lithium-Ion Batteries Using Multiple Virus Genes. *Science* **2009**, *324*, 1051−1055.

(30) Liu, Y.; Xu, Y.; Han, X.; Pellegrinelli, C.; Zhu, Y.; Zhu, H.; Wan, J.; Chung, A. C.; Vaaland, O.; Wang, C.; Hu, L. Porous Amorphous FePO₄ Nanoparticles Connected by Single-Wall Carbon Nanotubes for Sodium Ion Battery Cathodes. *Nano Lett.* **2012**, *12*, 5664−5668.

(31) Fang, Y.; Xiao, L.; Qian, J.; Ai, X.; Yang, H.; Cao, Y. Mesoporous Amorphous FePO₄ Nanospheres as High-Performance Cathode Material for Sodium-Ion Batteries. *Nano Lett.* **2014**, *14*, 3539−3543.

(32) Wang, Z.; Wang, Z.; Liu, W.; Xiao, W.; Lou, X. W. Amorphous CoSnO₃@C Nanoboxes with Superior Lithium Storage Capability. *Energy Environ. Sci.* **2013**, *6*, 87−91.

(33) Cui, L. F.; Ruffo, R.; Chan, C. K.; Peng, H.; Cui, Y. Crystalline Amorphous Core-Shell Silicon Nanowires for High Capacity and High Current Battery Electrodes. *Nano Lett.* **2009**, *9*, 491−495.

(34) Yi, R.; Feng, J.; Lv, D.; Gordin, M. L.; Chen, S.; Choi, D.; Wang, D. Amorphous Zn₂GeO₄ Nanoparticles as Anodes with High Reversible Capacity and Long Cycling Life for Li-Ion Batteries. *Nano Energy* **2013**, *2*, 498−504.

(35) Zhang, C.; Wang, X.; Liang, Q.; Liu, X.; Weng, Q.; Liu, J.; Yang, Y.; Dai, Z.; Ding, K.; Bando, Y.; Tang, J.; Golberg, D. Amorphous Phosphorus/Nitrogen-Doped Graphene Paper for Ultrastable Sodium-Ion Batteries. *Nano Lett.* **2016**, *16*, 2054−2060.

(36) Li, C.; Miao, X.; Chu, W.; Wu, P.; Tong, D. C. Hollow Amorphous NaFePO₄ Nanospheres as a High-Capacity and High-Rate Cathode for Sodium-Ion Batteries. *J. Mater. Chem. A* **2015**, *3*, 8265−8271.

(37) Liu, X.; Zhang, J.; Si, W.; Xi, L.; Oswald, S.; Yan, C.; Schmidt, O. G. High-Rate Amorphous SnO₂ Nanomembrane Anodes for Li-Ion Batteries with a Long Cycling Life. *Nanoscale* **2015**, *7*, 282−288.

(38) Zhao, K.; Liu, F.; Niu, C.; Xu, W.; Dong, Y.; Zhang, L.; Xie, S.; Yan, M.; Wei, Q.; Zhao, D.; Mai, L. Graphene Oxide Wrapped Amorphous Copper Vanadium Oxide with Enhanced Capacitive Behavior for High-Rate and Long-Life Lithium-Ion Battery Anodes. *Adv. Sci.* **2015**, *2*, No. 1500154.

(39) Liu, J.; Zheng, M.; Shi, X.; Zeng, H.; Xia, H. Amorphous FeOOH Quantum Dots Assembled Mesoporous Film Anchored on Graphene Nanosheets with Superior Electrochemical Performance for Supercapacitors. *Adv. Funct. Mater.* **2016**, *26*, 919−930.

(40) Owusu, K. A.; Qu, L.; Li, J.; Wang, Z.; Zhao, K.; Yang, C.; Hercule, K. M.; Lin, C.; Shi, C.; Wei, Q.; Zhou, L.; Mai, L. Low-Crystalline Iron Oxide Hydroxide Nanoparticle Anode for High-Performance Supercapacitors. *Nat. Commun.* **2017**, *8*, No. 14264.

(41) Yang, S.; Cao, C.; Huang, P.; Peng, L.; Sun, Y.; Wei, F.; Song, W. Sandwich-Like Porous TiO₂/reduced Graphene Oxide (rGO) for High-Performance Lithium-Ion Batteries. *J. Mater. Chem. A* **2015**, *3*, 8701−8705.

(42) Wang, Y. y.; Ni, Z. h.; Yu, T.; Shen, Z. X.; Wang, H. m.; Wu, Y. h.; Chen, W.; Wee, A. T. S. Raman Studies of Monolayer Graphene The Substrate Effect. *J. Phys. Chem. C* **2008**, *112*, 10637−10640.

(43) Yec, C. C.; Zheng, H. C. Nanobubbles within a Microbubble: Synthesis and Self-Assembly of Hollow Manganese Silicate and Its Metal-Doped Derivatives. *ACS Nano* **2014**, *8*, 6407−6416.

(44) Wang, C.; Yin, L.; Xiang, D.; Qi, Y. Uniform Carbon Layer Coated Mn₃O₄ Nanorod Anodes with Improved Reversible Capacity and Cyclic Stability for Lithium Ion Batteries. *ACS Appl. Mater. Interfaces* **2012**, *4*, 1636−1642.

(45) Cabana, J.; Monconduit, L.; Larcher, D.; Palacín, M. R. Beyond Intercalation-Based Li-Ion Batteries: The State of the Art and Challenges of Electrode Materials Reacting Through Conversion Reactions. *Adv. Mater.* **2010**, *22*, E170−E192.

(46) Zhou, L.; Wu, H. B.; Wang, Z.; Lou, X. W. Interconnected MoO₂ Nanocrystals with Carbon Nanocoating as High-Capacity Anode Materials for Lithium-ion Batteries. *ACS Appl. Mater. Interfaces* **2011**, *3*, 4853−4857.

(47) Yao, Y.; McDowell, M. T.; Ryu, I.; Wu, H.; Liu, N.; Hu, L.; Nix, W. D.; Cui, Y. Interconnected Silicon Hollow Nanospheres for

Lithium-Ion Battery Anodes with Long Cycle Life. *Nano Lett.* **2011**, *11*, 2949−2954.

(48) Noh, H.; Choi, W. Preparation of a TiNb₂O₇ Microsphere Using Formic Acid and Wrapping with Reduced Graphene Oxide for Anodes in Lithium Ion Batteries. *J. Electrochem. Soc.* **2016**, *163*, A1042−A1049.

(49) Kim, H. J.; Choi, S.; Lee, S. J.; Seo, M. W.; Lee, J. G.; Deniz, E.; Lee, Y. J.; Kim, E. K.; Choi, J. W. Controlled Prelithiation of Silicon Monoxide for High Performance Lithium-Ion Rechargeable Full Cells. *Nano Lett.* **2016**, *16*, 282−288.

(50) Zhao, H.; Wang, Z.; Lu, P.; Jiang, M.; Shi, F.; Song, X.; Zheng, Z.; Zhou, X.; Fu, Y.; Abdelbast, G.; Xiao, X.; Liu, Z.; Battaglia, V. S.; Zaghib, K.; Liu, G. Toward Practical Application of Functional Conductive Polymer Binder for a High-Energy Lithium-Ion Battery Design. *Nano Lett.* **2014**, *14*, 6704−6710.

(51) Liu, D.; Li, W.; Wan, F.; Fan, C.-Y.; Wang, Y.-Y.; Zhang, L.-L.; Lü, H.-Y.; Xing, Y.-M.; Zhang, X.-H.; Wu, X.-L. Restraining Capacity Increase To Achieve Ultrastable Lithium Storage: Case Study of a Manganese(II) Oxide/Graphene-Based Nanohybrid and Its Full-Cell Performance. *ChemElectroChem* **2016**, *3*, 1354−1359.

(52) Liu, D. H.; Lü, H. Y.; Wu, X. L.; Hou, B. H.; Wan, F.; Bao, S. D.; Yan, Q.; Xie, H. M.; Wang, R. S. Constructing the Optimal Conductive Network in MnO-Based Nanohybrids as High-Rate and Long-Life Anode Materials for Lithium-Ion Batteries. *J. Mater. Chem. A* **2015**, *3*, 19738−19746.

(53) Liu, D. H.; Lü, H. Y.; Wu, X. L.; Wang, J.; Yan, X.; Zhang, J. P.; Geng, H.; Zhang, Y.; Yan, Q. A New Strategy for Developing Superior Electrode Materials for Advanced Batteries: Using a Positive Cycling Trend to Compensate the Negative One to Achieve Ultralong Cycling Stability. *Nanoscale Horiz.* **2016**, *1*, 496−501.

(54) Zhang, F.; An, Y.; Zhai, W.; Gao, X.; Feng, J.; Ci, L.; Xiong, X. Nanotubes Within Transition Metal Silicate Hollow Spheres: Facile Preparation and Superior Lithium Storage Performances. *Mater. Res. Bull.* **2015**, *70*, 573−578.

(55) Han, M. H.; Gonzalo, E.; Singh, G.; Rojo, T. A Comprehensive Review of Sodium Layered Oxides Powerful Cathodes for Na-Ion Batteries. *Energy Environ. Sci.* **2015**, *8*, 81−102.

(56) Tu, F.; Xu, X.; Wang, P.; Si, L.; Zhou, X.; Bao, J. A Few-Layer SnS₂/Reduced Graphene Oxide Sandwich Hybrid for Efficient Sodium Storage. *J. Phys. Chem. C* **2017**, *121*, 3261−3269.